Journal of Materials Chemistry A

ROYAL SOCIETY OF CHEMISTRY

PAPER

View Article Online
View Journal | View Issue

Check for updates

Cite this: J. Mater. Chem. A, 2025, 13, 38858

Enhanced solubility and stability of active species in flow battery electrolytes *via* suppressed anthraquinone aggregation

Meysam Maleki and Marc-Antoni Goulet *

This study demonstrates that the cost-effective anthraquinones, such as alizarin and its derivative alizarin red S, can be promising for aqueous organic redox flow batteries (RFBs) by addressing their strong self-aggregation tendencies which typically result in low solubility and high capacity fade rates. This study shows that when alizarin and alizarin red S are mixed together, they exhibit suppression of aggregation which decreases these self-aggregation tendencies under alkaline conditions, resulting in enhancement of both the solubility and capacity retention of the mixture by 40% above the value expected from the rule of mixtures. By extending this approach to a ternary mixture of alizarin and alizarin red S with 2,6-DHAQ, this leads to a cost-effective electrolyte with a total concentration of stored electrons of 2.0 M and an OCV of 1.2 V at 50% state-of-charge, corresponding to a theoretical energy density of 64 Wh L^{-1} (one of the highest in anthraquinone-based electrolytes), which also demonstrates higher stability as a result of the same synergy between the redox-active compounds. These findings highlight how mixtures of redox active molecules can unexpectedly enhance the stability and energy density of organic RFBs through suppression of molecular aggregation while avoiding the added cost and complexity of molecular functionalization steps.

Received 27th July 2025
Accepted 7th October 2025

DOI: 10.1039/d5ta06073g

rsc.li/materials-a

Introduction

Renewable energy sources are an important aspect of a net zero future. However, while these sources are increasingly accessible, their intermittency remains a challenge.[1] To fully integrate renewable sources, excess renewable energy needs to be stored at large scale to balance supply and demand. Aqueous redox flow batteries (RFBs) offer a promising approach by storing energy in water-based electrolytes housed in external reservoirs, enabling the control of capacity and power output independently.[2] However, most commercial aqueous RFBs rely on vanadium which has a high and volatile price.[3,4] Moreover, their energy density is limited to <40 Wh L^{-1} due to the one-electron transfer reaction and aqueous solubility limit of vanadium.[5]

Redox-active organic compounds, like dihydroxyanthraquinones (DHAQs), have been developed as potential negolytes ('negative' or low potential electrolytes) in RFBs.[1] Among these, 2,6-DHAQ is one of the most well-investigated isomers from the DHAQ family,[6,7] with a theoretical energy density of ~38.5 Wh L^{-1} at its maximum solubility when paired with ferro-/ferricyanide as the posolyte ('positive' or high potential electrolyte).[8] However, its cost and capacity fade are still obstacles to its practical application.[9–11] Less expensive DHAQ isomers and derivatives on the other hand, may suffer from even higher capacity fade rates and solubility limitations, hindering their implementation in RFBs.[12,13] For instance, we previously demonstrated that the solubility of 1,2-DHAQ (alizarin) is limited to only ~0.2 M, corresponding to an energy density of 12 Wh L^{-1}.[14] Although the solubility of these molecules can be increased with chemical modifications,[15–17] these modifications can cause changes in other molecule characteristics, such as potential and stability.[18,19] For example, 2,6-DHAQ modified with bis(azanetriyl)tetrakis(propane-1-sulfonate) (2,6-N-TSAQ) exhibited remarkable cycling stability (0.025% per day), but at the cost of lower solubility (0.35 M, 0.25 M lower than unmodified 2,6-DHAQ).[20] In addition to such technical trade-offs, such modification-based approaches add associated synthesis costs. Another strategy for increasing the solubility and energy density of flow battery electrolytes has been through mixing of counterions,[21] or redox active species with similar potentials.[22] The energy density benefit of this mixed electrolyte approach was then demonstrated with organic species for a non-aqueous flow battery by Kosswattaarachchi and Cook in 2018.[23] More recently, Amini *et al.*[24] observed an energy density benefit from mixing anthraquinone species in the alkaline negolyte of an aqueous flow battery. A similar result was also observed in the 2024 study by Petrov *et al.*[25] on 2,7-anthraquinone disulfonic acid (2,7-AQDS) when mixed with 2,6-AQDS and 2-AQS in an acidic aqueous flow battery. Notably, both studies also report an improvement in capacity retention

Department of Chemical and Materials Engineering, Concordia University, Montreal, Quebec H3G 1M8, Canada. E-mail: marcantoni.goulet@concordia.ca

due to mixing, though without any further experimental investigation of the cause.

Herein, we demonstrate why the molecular mixing strategy for boosting solubility may also lead to an improvement in capacity fade rate beyond the expected weighted average. Our previous investigation on alizarin showed that the capacity fade of this electrolyte is primarily due to aggregation or precipitation of the molecule in the oxidized (discharged) form.[14] By mixing this compound with alizarin red S, a modified version of alizarin with a higher solubility limit and a slightly lower redox potential, we demonstrate a 40% improvement in both solubility and stability. This enhancement arises from suppression of aggregation between the two species and increases the lifespan and solubility limits. Importantly, we show that this effect is also present in a ternary mixture, further supporting its general applicability. This approach avoids the trade-offs of single-molecule modifications while providing a scalable path toward high-energy-density organic RFB electrolytes.

Results and discussion

The maximum practical solubilities of alizarin and alizarin red S (Fig. 1a) at pH 14 are about 0.2 and 0.3 M in KOH as the supporting electrolyte, respectively.[26] Maximum practical solubility was determined in two steps. First, a saturated solution was prepared, and the supernatant concentration was quantified by UV-vis spectroscopy (Fig. S1 for alizarin red S). Second, the saturated electrolyte was pumped through a flow cell; if the electrolyte was not flowable due to the excessive viscosity, the concentration was reduced until smooth flow was achieved. For

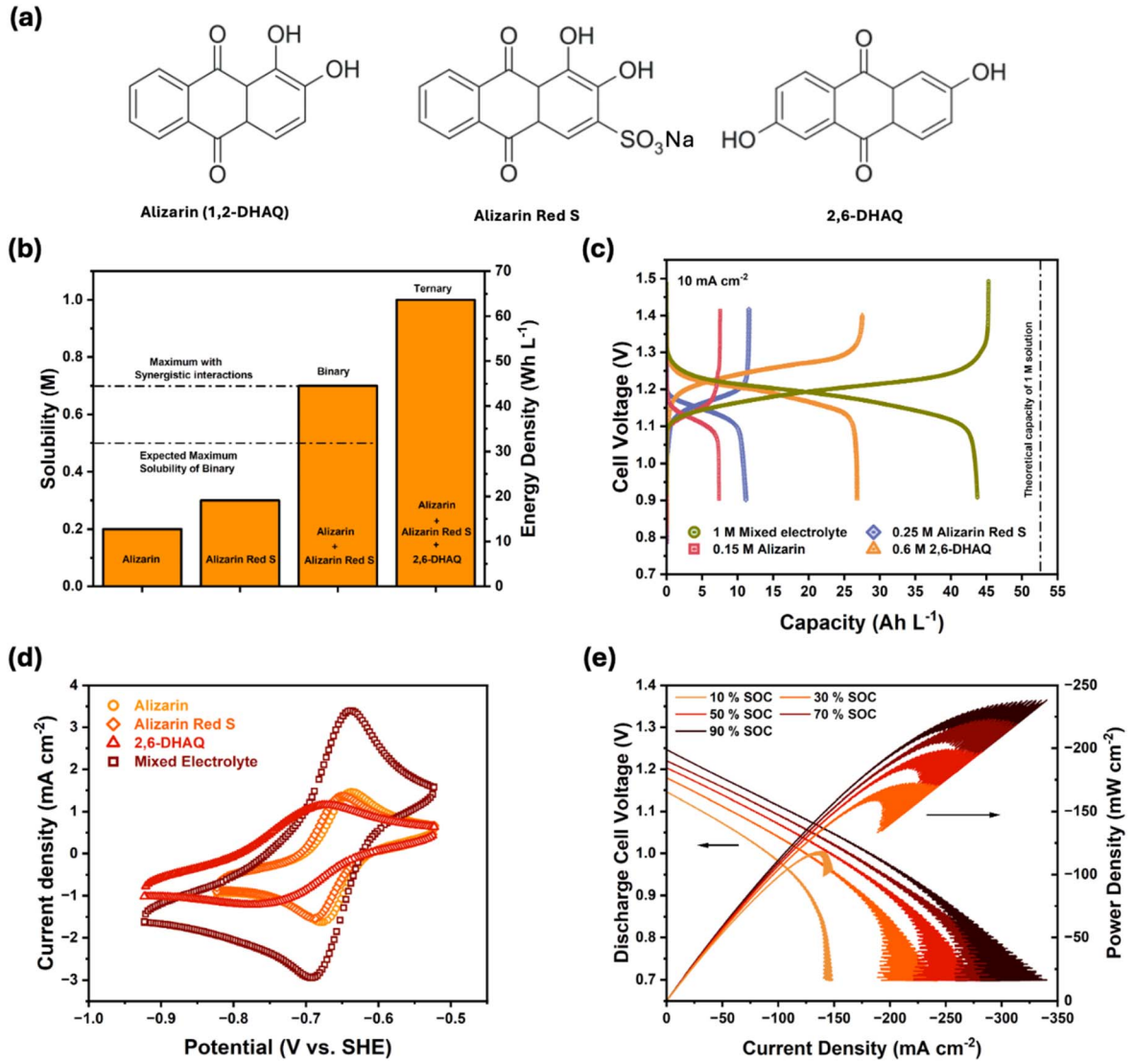

Fig. 1 (a) Chemical structures of alizarin, alizarin red S and 2,6-DHAQ. (b) Maximum practical solubility and corresponding energy density of single, binary, and ternary negolytes. (c) Galvanostatic charge and discharge curves at 10 mA cm^{-2} of single component and ternary negolyte–RFBs at their respective concentration in the ternary negolyte. (d) CV measurements of 10 mM alizarin, 10 mM alizarin red S, 10 mM 2,6-DHAQ and ternary electrolyte (1 : 1 : 1) with a scan rate of 100 mV s^{-1}. (e) Ternary negolyte–RFB polarization and corresponding power densities at different SOC values.

alizarin, the maximum practical solubility was determined from the flow test based on the solubility established in previous studies.[12,27] As illustrated in Fig. 1b, upon mixing the two anthraquinones (alizarin and alizarin red S) into the electrolyte, we expect a negolyte with a total concentration of 0.5 M (equivalent to 1 M of stored electrons). To confirm this, a flow cell was assembled using a binary mixture of 0.2 M alizarin + 0.3 M alizarin red S in 2 M KOH as the negolyte and ferro-/ferricyanide in 1 M KOH as the posolyte. Galvanostatic charge and discharge curves at 10 mA cm^{-2} yielded a capacity utilization of 86%, comparable to RFBs using either molecule individually (Fig. S2). To investigate the possibility of surpassing the individual solubility limits, a higher concentration was prepared with 0.3 M alizarin + 0.4 M alizarin red S in 2.4 M KOH, achieving a total concentration of 0.7 M. Despite exceeding the combined individual solubilities (0.5 M), this electrolyte exhibited a capacity utilization of 83% (Fig. 2e), indicating synergistic molecular interactions that enable enhanced solubility of both molecules.[28] It is worth mentioning that due to the close half-wave potential of the two compounds (~10 mV difference), the charge–discharge curves exhibit a single plateau, thereby mitigating the typical voltage inefficiency associated with separate redox events.[29] The mixed RFB showed a high voltage efficiency (VE) of 96%, comparable to, and even outperforming, other DHAQ-based RFBs.[30,31] Open circuit voltage (OCV) measurements show an increase in battery voltage compared to alizarin-RFB by 30 mV at 50% SOC, attributed to the more negative redox potential of alizarin red S (Fig. S3). The slightly larger OCV shift (~30 mV) compared to the ~10 mV half-wave potential difference measured by CV is likely due to a combination of small SOC discrepancies from the ideal 50% intended for the negolyte, and variation in the posolyte SOC between cells due to the time-dependent chemical reduction of ferricyanide to ferrocyanide.[32] A third compound, 2,6-DHAQ, was then added to the electrolyte to create a ternary mixture with 1 M of active species in 3 M KOH, to investigate its performance in the battery. A series of single component RFBs using alizarin, alizarin red S, and 2,6-DHAQ with corresponding concentrations in the ternary configuration were assembled as references (Fig. 1b). Capacity utilizations of ~86% were consistent across all systems. The OCV values at 50% SOC of alizarin (1.13 V), alizarin red S (1.15 V) and 2,6-DHAQ (1.25 V) align with the order of half-wave redox potentials measured with CV (Fig. 1c). The OCV value of the ternary cell at 50% SOC was measured to be 1.2 V (Fig. S4), slightly higher than that of the binary system of alizarin and alizarin red S at 1.16 V, due to the introduction of 2,6-DHAQ (1.25 V). This is consistent with the 1.21 V expected from a concentration-based weighted average. Generally, a higher molar fraction of the lower-potential compound is preferred in a negolyte, to maximize cell voltage, power and energy densities (Fig. 1d). At 64 Wh L^{-1}, the theoretical energy density of the ternary negolyte surpasses that of most anthraquinone-based RFBs (Table S1) and vanadium RFBs.[33] Additional cell performance data in the SI (Fig. S5 and S6) confirm that mixing of organic compounds does not compromise cell efficiency.

Prior to evaluating the stability of the mixed binary negolyte in a full cell, the individual stabilities of alizarin and alizarin red

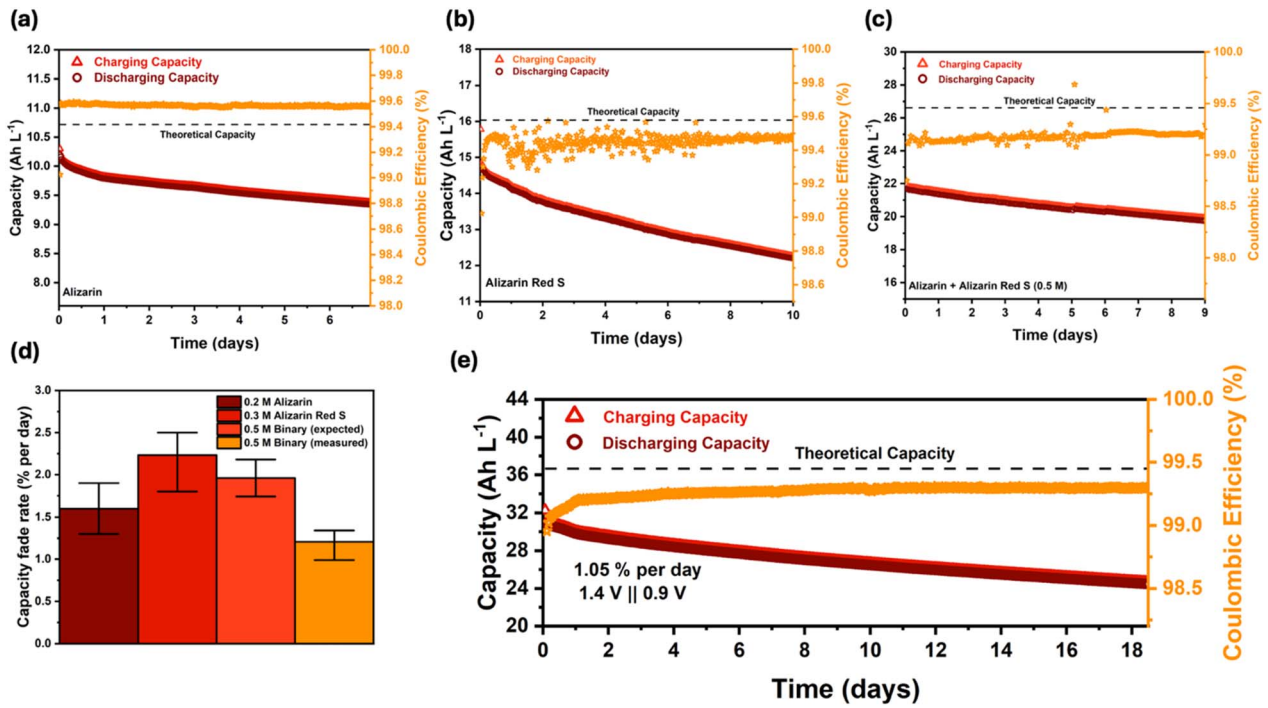

Fig. 2 Long-term RFB cycling tests of (a) 0.2 M alizarin in 1.4 M KOH, (b) 0.3 M alizarin red S in 1.6 M KOH, and (c) 0.5 M binary negolyte (0.2 M alizarin + 0.3 M alizarin red S) in 2 M KOH. (d) Capacity fade rate comparison of all cells with 3 repetitions for each battery. (e) Cycling of 0.7 M binary electrolyte (0.3 M alizarin + 0.4 M alizarin red S) in 2.4 M KOH. All cells were operated at pH 14, with Nafion 117 membranes and ferro–ferricyanide as the posolyte.

S were assessed at their maximum practical solubilities. Fig. 2a and b demonstrate that the capacity fade rate of alizarin is 1.6 ± 0.3% per day, while alizarin red S fades at the rate of 2.2 ± 0.3% per day. A comparison of capacity fade rates of the two compounds at different concentrations indicates that both compounds typically degrade more rapidly as concentration increases (Fig. S7), with this effect becoming more pronounced close to their practical solubility limits. We believe that for both molecules, a significant fraction of the capacity fade mechanism is linked to aggregation, leading to greater capacity fade rates at higher concentrations.[14] A comprehensive electrochemical and stability assessment of alizarin red S is provided in the SI (Fig. S8–S10). The capacity fade rate of each compound at its maximum practical solubility provides an estimate for the expected capacity fade rate of the mixed binary electrolyte (Note S1 and Fig. S7). Assuming a weighted average akin to the rule of mixtures, an RFB with an alizarin and alizarin red S negolyte mixed in a 2 : 3 ratio with a total concentration of 0.5 M in 2 M KOH, should experience a temporal fade rate of around 2.0 ± 0.2% per day. However, as shown in Fig. 2c, the measured capacity fade rate is only about 1.2 ± 0.2% per day, 40% lower than expected. Inspired by the unexpectedly longer lifespan, we implemented this approach with the 0.7 M mixed negolyte (0.3 M alizarin + 0.4 M alizarin red S) in 2.4 M KOH, representing a 40% solubility enhancement. As shown in Fig. 2e, the RFB cycling with this higher concentration negolyte for over 18 days displayed a capacity fade rate of about 1% per day, similar to the 0.5 M system. This observation further suggests that synergistic molecular interactions not only increase the solubility beyond individual limits but also mitigate aggregation-related capacity fade mechanisms.

To investigate the decomposition mechanism of the mixed electrolyte relative to its parent compounds, ^{1}H NMR analysis was conducted (Fig. S11). The comparison reveals that the degradation product peaks in the mixed electrolyte match the sum of those from alizarin and alizarin red S individually, indicating that the molecular interactions enhancing solubility do not alter their respective decomposition mechanisms. As a result, the lower capacity fade rate in the mixed electrolyte can be attributed to increased solubility limits for both compounds, which decreases capacity fade by reducing aggregation. To further validate that the decomposition products in the mixed electrolyte retain the characteristics of their parent compounds, an aliquot of the cycled electrolyte was exposed to air (Fig. S12). Within the precision of the NMR technique, the disappearance of degradation peaks upon oxygen exposure is similar to the observed behavior in other DHAQs,[10,14] further confirming that the underlying decomposition mechanisms remain unchanged.

Having established that the binary system exhibits improved solubility and stability, we next formulated a ternary electrolyte with a 1 M total concentration of redox active species in 3 M KOH by introducing a third anthraquinone, 2,6-DHAQ, into the binary system. Prior to the stability measurements of the ternary negolyte in a full cell, the long-term stability of its individual components was investigated at their respective concentrations. Fig. 3a–c demonstrate that the capacity fade rates of 0.6 M DHAQ in 2.2 M KOH, 0.15 M alizarin in 1.3 M KOH and 0.25 M alizarin red S in 1.5 M KOH are 1.33, 0.93 and 1.36% per day,

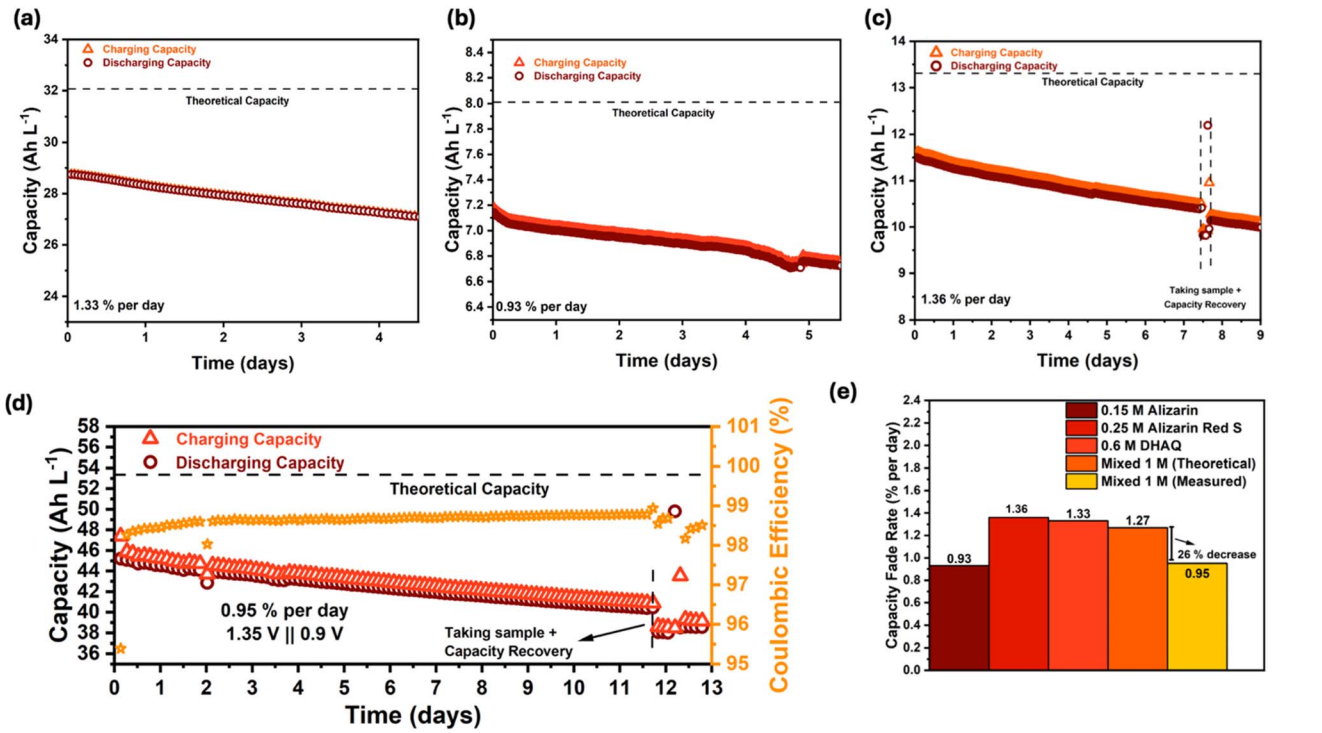

Fig. 3 Long-term RFB cycling stability tests of (a) 0.6 M 2,6-DHAQ in 2.2 M KOH, (b) 0.15 M alizarin in 1.3 M KOH, (c) 0.25 M alizarin red S in 1.5 M KOH, and (d) 1 M ternary negolyte (0.6 M 2,6-DHAQ + 0.15 M alizarin + 0.25 M alizarin red S) in 3 M KOH. All cells were operated at pH 14, with Nafion 117 membranes and ferro–ferricyanide as the posolyte. (e) Capacity fade rate comparison of all cells.

respectively. Based on a weighted average, the expected capacity fade rate for the ternary electrolyte would be 1.27% per day. However, when cycled in an RFB with ferro–ferricyanide as the posolyte, the measured fade rate was only 0.95% per day, a 26% improvement in stability, similar to that seen for the binary electrolyte.

This stability was further improved using the electrochemical regeneration strategy demonstrated by Jing *et al.*,[34] which involves applying low discharge voltages for electrochemical oxidation of degradation products (dimers) back into redox-active compounds. Some single DHAQ-based RFBs, including alizarin and 2,6-DHAQ, showed successful response to this recovery strategy.[14,35] We demonstrate here a similar capacity regeneration for alizarin red S (Fig. 3c and S10). This regeneration method was then implemented in an RFB with the ternary mixed electrolyte. As shown in Fig. 3d and S13, after ~12 days of cycling, an electrochemical regeneration step reduces the normal capacity fade rate by 0.16% per day. Implementing this strategy every 50 cycles over 10 days (Fig. S14) further reduced the full-cell capacity fade rate to 0.46% per day. It is worth mentioning that the deep discharge voltage was defined at 0.4 V to prevent excessive oxidation, since lower voltages oxidize both alizarin and alizarin red S into redox-inactive species, leading to permanent capacity lost (Fig. S15 and S16). The capacity recovered with this strategy suggests that all three compounds inside the electrolyte are being regenerated similarly to the single anthraquinone RFBs.

To understand the enhanced solubility and stability in the mixed negolytes, the intermolecular interactions were first studied in the binary mixture. Fig. 4a presents the ^{1}H NMR spectra of alizarin + alizarin red S at different concentrations, but with a constant 2 : 3 molar ratio equal to that used in the battery. Increasing the concentration shifts the multiplet peaks by 0.024 ppm around 7.5–7.6 ppm upfield (from 7.534 ppm for 10 mM solution to 7.510 ppm for 100 mM solution), indicating changes in the local electronic environment.[36] Furthermore, peak broadening around 8.0 ppm indicates intermolecular interactions that affect molecular movement.[37] Notably, the NMR spectra at all concentrations display no evidence of new chemical species, confirming that the observed interactions arise from non-covalent molecular forces rather than chemical reactions. These interactions were further investigated using COSY NMR spectroscopy (Fig. S17), where the comparison of mixed and single-component electrolyte (alizarin) reveals no

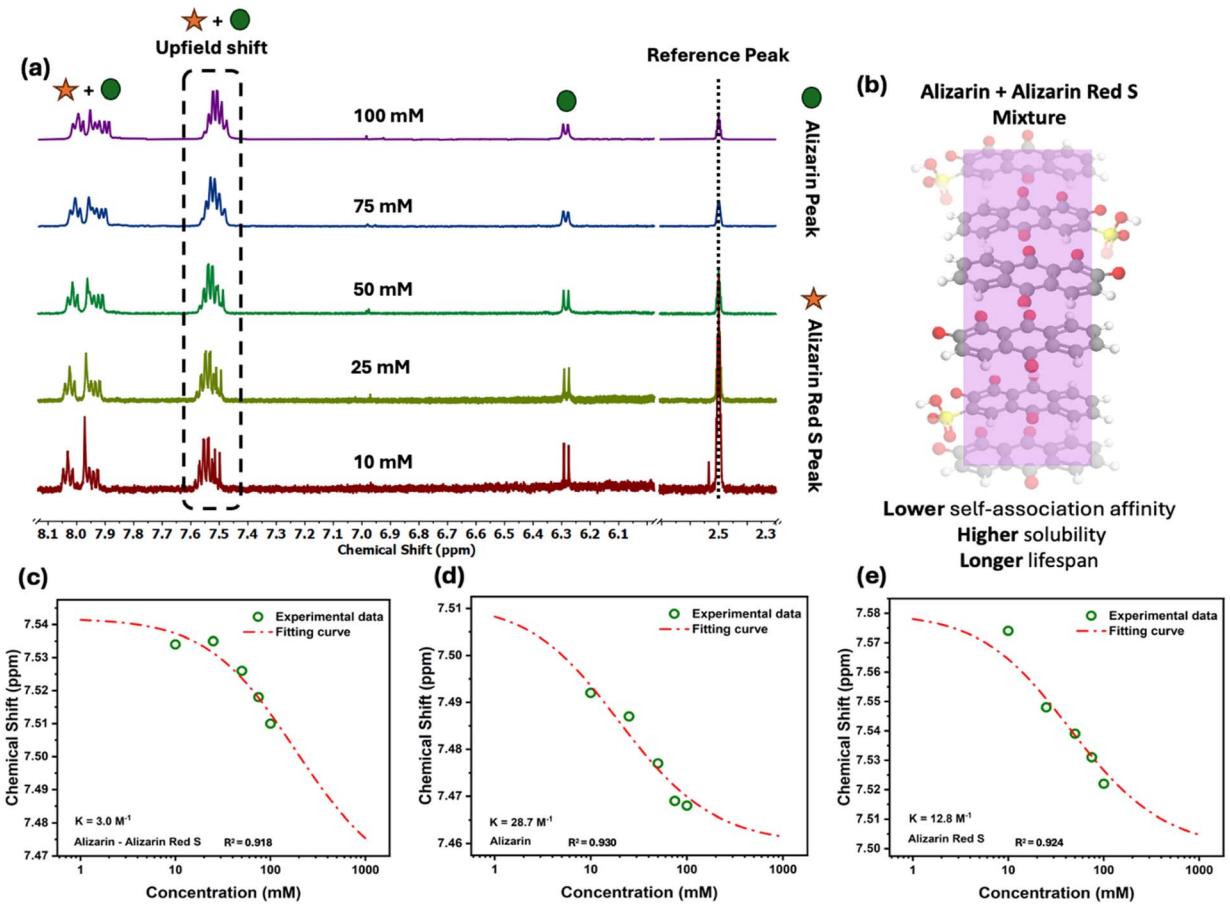

Fig. 4 Intermolecular interactions studies. (a) ^{1}H NMR spectra of alizarin + alizarin red S electrolyte with different concentrations at a fixed molar ratio used in stability measurement (40% alizarin + 60% alizarin red S) in D_2O with DMSO-d_6 as the internal reference. (b) Representation of possible aggregation between alizarin and alizarin red S. Chemical shift of multiplet peaks *versus* concentration of electrolyte in (c) alizarin + alizarin red S, (d) alizarin and (e) alizarin red S.

new cross-peaks, confirming that there was no chemical reaction upon mixing. This finding is further supported by LC-MS analysis, where spectra of the freshly prepared binary electrolyte (Fig. S18) and those stored for 7 days (Fig. S19) show no evidence of new compound formation. Fig. 4b schematically illustrates a possible arrangement of alizarin red S and alizarin molecules which would disturb the π–π stacking between each molecule, consistent with the reduced binding affinity observed.

To systematically investigate the molecular interactions between alizarin and alizarin red S, we examined the chemical shift of multiplet peaks *versus* concentration of electrolyte (Fig. 4c–e). The experimental NMR data (Fig. 4a and S20) were fitted using the isodesmic model (Note S2), which describes stepwise molecular interactions with a constant binding affinity at each stacking step.[38] The model yielded a binding constant of $K = 3.0\ M^{-1}$ between the two compounds. In contrast, the self-association measurements of alizarin and alizarin red S revealed much higher binding constants of 28.7 and 12.8 M^{-1} respectively, indicating substantially stronger π–π interactions that lead to the lower solubility of each compound when being used as a single compound in the electrolyte. The lower binding affinity observed in the binary mixture suggests that the presence of alizarin red S effectively disrupts the strong self-association of alizarin, and *vice versa*. In addition to entropic effects on the crystallization energy, this disruption of initial aggregation is likely due to the SO_3^- functional group on alizarin red S, which modifies the local electrostatic environment, thereby reducing the overall binding strength between aromatic units. Increased solubility driven by non-covalent interactions has been reported for organic molecules, such as 9,10-anthraquinone-2,7-disulfonic acid (AQDS) interacting with NH_4^+ ion and hydroquinone (HQ) interacting with hydrotropic species in the supporting electrolyte.[39,40] However, in these cases, the species interacting with the organic molecule did not function as an additional redox-active component, and thus did not contribute to further enhancement of the energy density of battery. In addition to the electrostatic effect from the negatively charged sulfonate group of alizarin red S, it can also introduce steric hindrance that physically disrupts the strong π–π stacking of the anthraquinone cores.[41] The small binding affinity of the alizarin + alizarin red S mixture not only increases the solubility and energy density of the electrolyte but also mitigates its primary failure mode by reducing the aggregation rate, thereby enhancing battery lifetime. Apart from decreasing aggregation rate, mixing different redox-active species can, in some cases, influence other degradation pathways. For example, Lee *et al.*,[42] recently demonstrated that incorporating 4,4′-((9,10-anthraquinone-2,6-diyl)dioxy)dibutyrate (DBEAQ) into a 2,6-DHAQ electrolyte enabled regeneration of DHAQ from its anthrone and dimer degradation products, lowering the fade rate beyond the rule of mixtures prediction. In our system, however, previous work has shown that aggregation accounts for the overwhelming majority of capacity fade (~92%), whereas disproportionation and dimerization together contribute about 5%.[14] Consistent with this, we observe a 40% reduction in the fade rate and a clear increase in solubility when alizarin and alizarin red S are mixed. These observations indicate that, unlike the chemical–electrochemical regeneration pathway in the DHAQ/DBEAQ system, the stabilizing effect here arises mainly from the suppression of aggregation as a result of mixing compounds.

Due to the substantial benefits listed above, we further investigated whether a ternary mixture with the third anthraquinone, 2,6-DHAQ, exhibits the same solubility and stability enhancement due to similarly improved hydration and tuned π–π stacking interactions. First, we conducted ^1H NMR experiments on binary combinations, 2,6-DHAQ–alizarin and 2,6-DHAQ–alizarin red S (Fig. S21). In both cases, the proton peaks of 2,6-DHAQ shift downfield when interacting with alizarin or alizarin red S without new appeared peaks, demonstrating the non-covalent interactions and changes in electronic environments. However, the shifts of 2,6-DHAQ peaks were more pronounced ($\Delta\delta_{DHAQ\text{–alizarin red S}} = 0.045$ ppm *vs.* $\Delta\delta_{DHAQ\text{–alizarin}} = 0.023$ ppm) when interacting with alizarin red S, which may be due to the strong electron withdrawing effect of the SO_3^- group of alizarin red S as reported by Gerhardt *et al.*[18] Upon the introduction of 2,6-DHAQ into the binary system, 2,6-DHAQ peaks exhibited a downfield shift, indicating its interaction with the other compounds (Fig. S22). As in the binary mixture, we believe these interactions to be responsible for the improved solubility seen in Fig. 1a and the improved stability seen in Fig. 3e.

Conclusions

This study demonstrates the impact of molecular interactions on the solubility and stability of anthraquinone-based electrolytes for aqueous RFBs. In the binary mixture, alizarin and alizarin red S exhibited synergistic interactions, where their combined presence enhanced both solubility and stability by mitigating the strong self-aggregation phenomenon seen in alizarin and alizarin red S. Then, 2,6-DHAQ was introduced into the system to examine whether the presence of a third redox-active species shows similar synergistic interactions. The resulting ternary electrolyte is formulated with a total redox-active concentration of 1 M with an OCV of 1.2 V at 50% SOC, corresponding to the one of the highest energy densities (64 Wh L^{-1}) in anthraquinone-based RFBs. In addition, this mixture leads to a decrease in the expected capacity fade rate based on the rule of mixtures. These benefits were achieved using cost-effective and commercially available anthraquinones without the additional cost of molecular functionalization steps. These findings highlight the possibility of using redox active mixtures as a promising pathway to exceed the current limits on the energy density and lifetime of flow battery electrolytes.

Author contributions

MM and MAG conceived the idea. MM performed experimental work. MAG supervised the project. Both authors wrote and edited the manuscript.

Conflicts of interest

The authors declare the following competing financial interest: Marc-Antoni Goulet has minor ownership stakes in Quino Energy, Inc., which may profit from the results reported in this study.

Data availability

Primary data for this article, including all numerical values for figures, are available as spreadsheets hosted at Zenodo data repository. See DOI: **https://doi.org/10.5281/zenodo.16507257**.

Supplementary information: additional data supporting the conclusions of the study. See DOI: **https://doi.org/10.1039/d5ta06073g**.

Acknowledgements

The authors would like to acknowledge Dr Constantin Yannopoulos of the NMR Facility and Prof. Marek Majewski in the Department of Chemistry and Biochemistry of Concordia University for NMR support and insights. Similarly, we would like to acknowledge Prof. Kiana Amini at the University of British Columbia, and Prof. Johan Hjelm at the *Danmarks Tekniske Universitet* for helpful discussions. Lastly, we acknowledge the funding support from Fonds de Recherche du Québec Nature et Technologies (FRQNT) – Strategic Clusters (RS-265155) and Établissement de la relève professorale (325551).

Notes and references

1 G. Yang, Y. Zhu, Z. Hao, Y. Lu, Q. Zhao, K. Zhang and J. Chen, *Adv. Mater.*, 2023, **35**, 2301898.
2 Y. Yao, J. Lei, Y. Shi, F. Ai and Y.-C. Lu, *Nat. Energy*, 2021, **6**, 582–588.
3 D. Emmel, S. Kunz, N. Blume, Y. Kwon, T. Turek, C. Minke and D. Schröder, *Nat. Commun.*, 2023, **14**, 6672.
4 K. E. Rodby, R. L. Jaffe, E. A. Olivetti and F. R. Brushett, *J. Power Sources*, 2023, **560**, 232605.
5 M. Shoaib, P. Vallayil, N. Jaiswal, P. Iyapazham Vaigunda Suba, S. Sankararaman, K. Ramanujam and V. Thangadurai, *Adv. Energy Mater.*, 2024, **14**, 2400721.
6 E. W. Zhao, T. Liu, E. Jónsson, J. Lee, I. Temprano, R. B. Jethwa, A. Wang, H. Smith, J. Carretero-González, Q. Song and C. P. Grey, *Nature*, 2020, **579**, 224–228.
7 E. W. Zhao, E. Jónsson, R. B. Jethwa, D. Hey, D. Lyu, A. Brookfield, P. A. A. Klusener, D. Collison and C. P. Grey, *J. Am. Chem. Soc.*, 2021, **143**, 1885–1895.
8 K. Lin, Q. Chen, M. R. Gerhardt, L. Tong, S. B. Kim, L. Eisenach, A. W. Valle, D. Hardee, R. G. Gordon, M. J. Aziz and M. P. Marshak, *Science*, 2015, **349**, 1529–1532.
9 M.-A. Goulet and M. J. Aziz, *J. Electrochem. Soc.*, 2018, **165**, A1466–A1477.
10 M.-A. Goulet, L. Tong, D. A. Pollack, D. P. Tabor, S. A. Odom, A. Aspuru-Guzik, E. E. Kwan, R. G. Gordon and M. J. Aziz, *J. Am. Chem. Soc.*, 2019, **141**, 8014–8019.
11 A. Sahoo and K. Ramanujam, *J. Mater. Chem. A*, 2023, **11**, 13623–13632.
12 J. Cao, M. Tao, H. Chen, J. Xu and Z. Chen, *J. Power Sources*, 2018, **386**, 40–46.
13 M. Wu, M. Bahari, E. M. Fell, R. G. Gordon and M. J. Aziz, *J. Mater. Chem. A*, 2021, **9**, 26709–26716.
14 M. Maleki, S. Imhanria, L. Duguet and M.-A. Goulet, *J. Electrochem. Soc.*, 2024, **171**, 120537.
15 K. Amini, E. F. Kerr, T. Y. George, A. M. Alfaraidi, Y. Jing, T. Tsukamoto, R. G. Gordon and M. J. Aziz, *Adv. Funct. Mater.*, 2023, **33**, 2211338.
16 Y. Jing, E. M. Fell, M. Wu, S. Jin, Y. Ji, D. A. Pollack, Z. Tang, D. Ding, M. Bahari, M.-A. Goulet, T. Tsukamoto, R. G. Gordon and M. J. Aziz, *ACS Energy Lett.*, 2022, **7**, 226–235.
17 Y. Wang, H. Hong, Z. Wei, X. Yang, D. Li, S. Wang and C. Zhi, *Adv. Funct. Mater.*, 2025, 2507320.
18 M. R. Gerhardt, L. Tong, R. Gómez-Bombarelli, Q. Chen, M. P. Marshak, C. J. Galvin, A. Aspuru-Guzik, R. G. Gordon and M. J. Aziz, *Adv. Energy Mater.*, 2017, **7**, 1601488.
19 J. Huang, B. Pan, W. Duan, X. Wei, R. S. Assary, L. Su, F. R. Brushett, L. Cheng, C. Liao, M. S. Ferrandon, W. Wang, Z. Zhang, A. K. Burrell, L. A. Curtiss, I. A. Shkrob, J. S. Moore and L. Zhang, *Sci. Rep.*, 2016, **6**, 32102.
20 M. Wu, M. Bahari, Y. Jing, K. Amini, E. M. Fell, T. Y. George, R. G. Gordon and M. J. Aziz, *Batteries Supercaps*, 2022, **5**, e202200009.
21 A. J. Esswein, J. Goeltz and D. Amadeo, *US Pat.*, US9997799B2, 2018.
22 S. Park, H. J. Lee, H. Lee and H. Kim, *J. Electrochem. Soc.*, 2018, **165**, A3215.
23 A. M. Kosswattaarachchi and T. R. Cook, *J. Electrochem. Soc.*, 2018, **165**, A194.
24 K. Amini, Y. Jing, J. Gao, J. D. Sosa, R. G. Gordon and M. J. Aziz, *J. Electrochem. Soc.*, 2023, **170**, 120535.
25 M. M. Petrov, D. V. Chikin, K. A. Karpenko, L. Z. Antipova, P. A. Loktionov, R. D. Pichugov, A. R. Karastsialiova, A. N. Vereshchagin and A. E. Antipov, *J. Electroanal. Chem.*, 2024, **973**, 118693.
26 S. Guiheneuf, A. Lê, T. Godet-Bar, L. Chancelier, J. Fontmorin, D. Floner and F. Geneste, *ChemElectroChem*, 2021, **8**, 2526–2533.
27 S. Huang, H. Zhang, M. Salla, J. Zhuang, Y. Zhi, X. Wang and Q. Wang, *Nat. Commun.*, 2022, **13**, 4746.
28 X. Yang, G. Lu, K. Huang, R. Wang, X. Duan, C. Yang, H. Yin and Z. Dang, *J. Mol. Liq.*, 2016, **223**, 252–260.
29 C. M. Davis, S. E. Waters, B. H. Robb, J. R. Thurston, D. Reber and M. P. Marshak, *Batteries*, 2023, **9**, 573.
30 S. Jin, Y. Jing, D. G. Kwabi, Y. Ji, L. Tong, D. De Porcellinis, M.-A. Goulet, D. A. Pollack, R. G. Gordon and M. J. Aziz, *ACS Energy Lett.*, 2019, **4**, 1342–1348.
31 S. Guiheneuf, T. Godet-Bar, J.-M. Fontmorin, C. Jourdin, D. Floner and F. Geneste, *J. Power Sources*, 2022, **539**, 231600.
32 E. M. Fell, D. D. Porcellinis, Y. Jing, V. Gutierrez-Venegas, T. Y. George, R. G. Gordon, S. Granados-Focil and M. J. Aziz, *J. Electrochem. Soc.*, 2023, **170**, 070525.

33 L. Li, S. Kim, W. Wang, M. Vijayakumar, Z. Nie, B. Chen, J. Zhang, G. Xia, J. Hu, G. Graff, J. Liu and Z. Yang, *Adv. Energy Mater.*, 2011, **1**, 394–400.
34 Y. Jing, E. W. Zhao, M.-A. Goulet, M. Bahari, E. M. Fell, S. Jin, A. Davoodi, E. Jónsson, M. Wu, C. P. Grey, R. G. Gordon and M. J. Aziz, *Nat. Chem.*, 2022, **14**, 1103–1109.
35 M. Bahari, Y. Jing, S. Jin, M.-A. Goulet, T. Tsukamoto, R. G. Gordon and M. J. Aziz, *ACS Appl. Mater. Interfaces*, 2024, **16**, 52144–52152.
36 K. Peng, Y. Li, G. Tang, Y. Liu, Z. Yang and T. Xu, *Energy Environ. Sci.*, 2023, **16**, 430–437.
37 D. A. Middleton, *Prog. Nucl. Magn. Reson. Spectrosc.*, 2024, **144–145**, 63–96.
38 T. J. Carney, S. J. Collins, J. S. Moore and F. R. Brushett, *Chem. Mater.*, 2017, **29**, 4801–4810.
39 B. Hu, J. Luo, M. Hu, B. Yuan and T. L. Liu, *Angew. Chem.*, 2019, **131**, 16782–16789.
40 J. Byeon, J. Ko, S. Lee, D. H. Kim, S. W. Kim, D. Kim, W. Oh, S. Hong and S. J. Yoo, *ACS Energy Lett.*, 2023, **8**, 2345–2355.
41 E. S. Beh, D. De Porcellinis, R. L. Gracia, K. T. Xia, R. G. Gordon and M. J. Aziz, *ACS Energy Lett.*, 2017, **2**, 639–644.
42 K. Lee, K. Amini and M. J. Aziz, *ACS Energy Lett.*, 2025, **10**, 4067–4073.